WILEY | Hindawi

Research Article

Damage Characteristic of Thermal Shock on the Physical and Dynamic Compressive Properties of Granite

Ronghua Shu [1,2] **Lijinhong Huang** [3,4] **Xueyi Zhi,**[1] **Zhenyu Han,**[5,6] **Yuzhang Lai,**[1] **Huizhen Li,**[1] **and Chun Wang** [7]

[1]*School of Resources and Environmental Engineering, Jiangxi University of Science and Technology, Ganzhou 341000, China*
[2]*Engineering Research Center for High-efficiency Development and Application Technology of Tungsten Resources (Jiangxi University of Science and Technology), Ministry of Education, Ganzhou 341000, China*
[3]*School of Architecture and Design, Jiangxi University of Science and Technology, Ganzhou 341000, China*
[4]*Faculty of Science and Engineering, WA School of Mines: Minerals, Energy, and Chemical Engineering, Curtin University, WA 6150, Australia*
[5]*School of Civil Engineering, Southeast University, Nanjing 210096, China*
[6]*Department of Civil Engineering, Monash University, Melbourne, Victoria 3800, Australia*
[7]*School of Energy Science and Engineering, Henan Polytechnic University, Jiaozuo 454003, China*

Correspondence should be addressed to Lijinhong Huang; angeline777@sina.com and Chun Wang; wczy115728@163.com

Thermal shock is common in fire disaster and blasting of rock engineering; moreover, the rock mass bears dynamic mechanical disturbance frequently. In order to study the damage characteristics of thermal shock on physical and dynamic compressive properties, the thermal shock damage of granite treated to different temperatures at different heating rates was obtained by measure the ultrasonic wave velocity, and the internal structures were obtained by scanning electron microscopy experiments. By using split Hopkinson pressure bar, the dynamic experiments on granite treated to 400°C and 600°C at heating rates of 1, 2, 4, 6, 10, 20, 30, and 40°C/min were carried out. Thereby, the damage characteristics of thermal shock on the physical and dynamic compressive properties of granite were obtained. The results show that there is a heating rate threshold value between 6 and 10°C/min, which divides the thermal shock damage. Before the threshold value, the thermal shock does not appear. The dynamic compressive strength, dynamic elastic modulus, and density decrease; however, peak strain increases as the thermal shock damage increases. The researches of thermal effect on granite by heating with the heating rate below or equal to 6°C/min could avoid thermal shock. The research could provide a theoretical foundation for rock engineering suffered thermal shock, such as geothermal reservoir.

1. Introduction

Recently, thermal effect on rock properties including physical and mechanical properties has become into one of hot topics in rock engineering for researchers [1–7]. Study of thermal effect on physical and mechanical properties is critical for many rock applications, such as deep mining, rock drilling, ore crushing [8], development and utilization of geothermal energy [9], geological disposal of nuclear waste [10–12], and the protection of buildings (over ground and underground buildings) against fire or building restoration and reconstruction after fire [13, 14]. In fact, most of rock engineering, which is related to temperature, could subject to thermal shock caused by blasting, fire, different thermal gradients, and nuclear radiation. In addition, most of rock engineering, which is connected to temperature, could also suffered dynamic disturbance due to drilling, blasting, and earthquake. Hence, to investigate the damage characteristic of thermal shock on the physical properties and dynamic properties of granite, which could offer a strong theoretical

support and guidance for design, stability evaluation and restoration of rock engineering, is urgent and highly significant.

Investigations of thermal effect on physical properties of rocks are mainly concentrated on density and porosity [15, 16]. The conclusions nearly conformed as follows: the density decreases with the increasing temperature; the opposite phenomenon comes to porosity. And the researches of thermal effect on dynamic properties of rocks are primarily focused on dynamic strength and elastic modulus [17–23]. The scholars conducted that when the temperature increases, the dynamic strength and elastic modulus all decrease with different degrees which is related to the rock materials. All of them just heated the rock specimens at a low heating rate to avoid thermal shock. Nevertheless, the thermal shock is common in deep rock engineering, such as deep mining and geothermal energy extraction. When the exploitation depth increases, the temperature increases with different geothermal gradients varying from 30 to 50°C/km due to the different hydrogeology and existing conditions, which could cause thermal shock and finally change the value of stress in the rock mass. It is worth noting that the geothermal gradient can be very high, even reaching about 100°C/km in some specific places. Besides, the thermal shock also occurs in blasting, fire, and nuclear radiation. Considering on the fact of thermal shock in many rock engineering, some researchers have involved in the heating rate effect on the physical and mechanical properties of rocks. For example, by carried out the experiments on granites which were heated with different heating rates (5°C/min, 20°C/min, and 50°C/min) to different temperatures (20-400°C), Thirumalai et al. [24] point out that thermal effect enhances accordingly with the increasing heating rate at the same temperature, namely, the thermal expansion increases gradually as the heating rate increases. Richter et al. [25] showed the same phenomenon by carrying out an experiment on gabbro heated to 300°C with heating rates of 1 and 5°C/min, respectively. That is, the higher the heating rate, the larger the expansion coefficient. By carried out experiments, Yong et al. [26] show that the heating rate is one of the important factors affecting the rock properties. In addition, Li et al. [27] performed tests in dynamic tensile mechanical properties of coal sandstone under 800°C high temperature and therewith the rapid cooling at different heating rates and state that the dynamic tensile properties of sandstone gradually decrease with increasing heating rate. They emphasize that the heating rate is the key factor making a large difference to investigation of the mechanical properties of materials, which can both significantly affected the crystal texture or recombination and influenced the macroscopic mechanical properties of rocks. The thermal shock effect on the physical and mechanical properties of rocks could though out the experiment on rocks heated to different heating rates.

Although there are some scholars have researched the heating rate effect on physical and mechanical properties of rocks, they only focused on physical properties, static properties, and dynamic tensile mechanical properties. The thermal shock on the dynamic compressive properties of rocks is neglected; moreover, none of them studied from the point view of damage. Hence, in order to put forward a strong the-
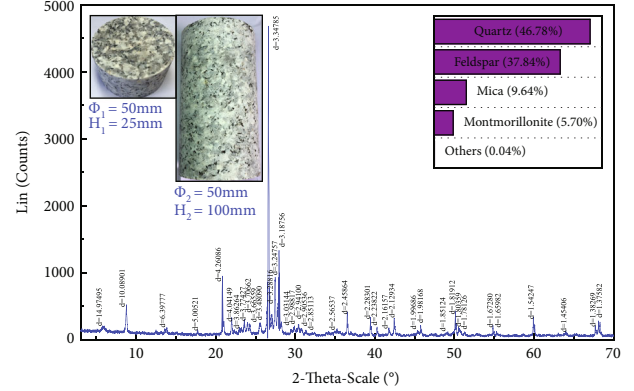

Figure 1: The components and appearances of granite specimens at room temperature.

Table 1: The basic physical and mechanical properties of granite specimen.

Rock type	ρ (kg/m^3)	σ_s (MPa)	E (GPa)	V (m/s)
Granite	2546.72	102.83	25.06	4183.95

(note: ρ, σ_s, E, and V stands for the density, static compressive strength, static elastic modulus, and P-wave velocity, respectively.).

oretical foundation and guidance for design, stability evaluation and restoration of rock engineering and make an insight understanding on the damage characteristic of thermal shock on the physical and dynamic compressive properties of granite; in this paper, the dynamic experiments on granite specimens heated to different temperatures (400°C and 600°C) with different heating rates (1°C/min, 2°C/min, 4°C/min, 6°C/min, 10°C/min, 20°C/min, 30°C/min, and 40°C/min). The damage characteristic of thermal shock on the physical and dynamic compressive properties of granite was analyzed and discussed, which was involved in the density, dynamic compressive strength, peak strain, and dynamic elastic modulus.

2. Laboratory Experiment

2.1. Specimen Preparation. To avoid any variation due to natural anisotropy of specimens, the tested granite specimens were cored from the same rock blocks obtained in Changsha, China. There are no distinct layering, laminations or flaws observed in the specimen surface, and the granite specimen consists of 46.78% quartz, 37.84% feldspar, 9.64% mica, 5.70% montmorillonite, and 0.04% other components, as shown in Figure 1. According to the requirements of the rock mechanical testing procedures suggested by the ISRM [28], the granite specimens used here were processed into a cylinder with dimensions of Φ 50 mm × 100 mm and a cylinder with dimensions of Φ 50 mm × 25 mm, which are used for static and dynamic test, respectively. Particularly, in order to ensure their parallelism, flatness, and finish, both ends of the specimens were polished, controlling the parallelism within ±0.05 mm and the surface flatness within ±0.02 mm. Furthermore, the P-wave velocity of polished specimen was measured
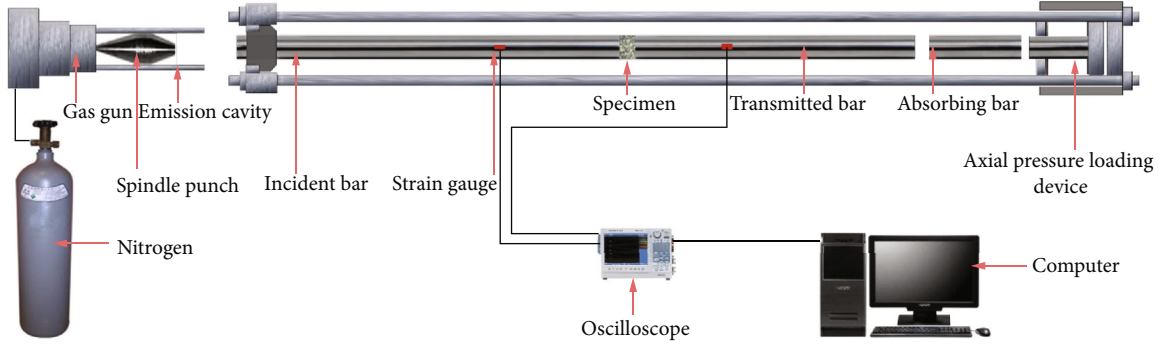
Figure 2: The split Hopkinson pressure bar system.
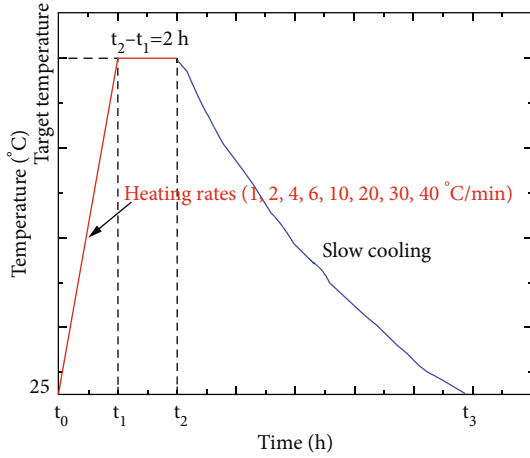

Figure 3: The heating and cooling methods.

by using a rock and soil engineering quality detector, and then specimens of similar P-wave velocities were selected in order to guarantee the reliability of the experiment. The basic physical and static mechanical properties of specimen are given as Table 1.

2.2. Test Apparatus. The main test apparatus used here is variable-speed heating furnace, scanning electron microscopy, electrohydraulic and servo-controlled material testing machine, and split Hopkinson pressure bar. The variable-speed heating furnace, which consists of a heating cabinet and smart controller, is designed to have a rated power of 4 kW, a maximum temperature of 1200°C, and a maximum heating rate of 40°C/min. The scanning electron microscope of type EVO-MA10 is used to obtain the internal structure of rock specimen. The electrohydraulic and servo-controlled material testing machine (Instron 1346) mainly consists of main body (a pressure device, compression bar, strut bars, and support) and a control and data-processing device. The split Hopkinson pressure bar consists of a spindle punch, an emission cavity, a gas gun, an incident bar (φ 50 mm × 2000 mm), a transmission bar (φ 50 mm × 1500 mm), an absorbing bar (φ 50 mm × 500 mm), a signal recording device including high dynamic strain indicator, and oscilloscope. The ultimate strength, wave velocity, elastic modulus, Poisson's ratio, and

density of the bar are 800 MPa, 5400 m/s, 240 GPa, 0.28, and 7810 kg/m³, respectively, as shown in Figure 2. The complete stress–strain curve could be obtained due to the higher stiffness of the high-strength alloy bar compared to that of the rock specimen. The resistance strain gauges are bonded to the incident bar and the transmitted bar, respectively, to record the voltage signals. The distance between the strain gauge and the end face of the test bar is 1004 mm for both the incident and the transmission bar. In addition, a stable strain rate of half the sinusoidal stress wave is produced by a spindle punch [29]. The incident, reflected, and transmitted waves are measured by the signals recorded through strain gauges fixed on the incident and transmitted bars. Correspondently, the stress σ (t), strain ε (t), and strain rate $\dot{\varepsilon}$ (t) could be calculated from the cross-sectional area A_S of the specimen, the cross-sectional area A_0 of the pressure bar, the wave velocity C_0 of the pressure bar, the elastic modulus E_0 of bar, the length L_S of the rock specimen, the incident strain ε_P, the reflected strain ε_R, and the transmitted strain ε_T, by using Formula (1).

$$
\begin{cases}
\sigma(t) = \dfrac{A_0}{2A_S} E(\varepsilon_I + \varepsilon_R + \varepsilon_T), \\
\varepsilon(t) = \dfrac{C_0}{L_S} \displaystyle\int_0^t (\varepsilon_I - \varepsilon_R - \varepsilon_T) dt, \\
\dot{\varepsilon}(t) = \dfrac{C_0}{L_S} (\varepsilon_I - \varepsilon_R - \varepsilon_T).
\end{cases}
\tag{1}
$$

2.3. Experimental Method. For X-ray diffraction and static experiments, the number of specimens should be no less than three. For dynamic experiment, consideration on α-β transition of quartz at around 573°C [30], the granite specimens are divided into three large groups: one group for heated (0°C/min), the second group are heated to 400°C, heating rates of which are 1, 2, 4, 6, 10, 20, 30, and 40°C/min, and the last group are heated to 600°C, heating rates of which are 1, 2, 4, 6, 10, 20, 30, and 40°C/min. According to the divided groups, the specimens are numbered accordingly. Before thermal treatment, the basic properties of granite specimens, including static compressive strength, density, ultrasonic wave velocity, and static elastic modulus, should be measured no less than three times. Then, the
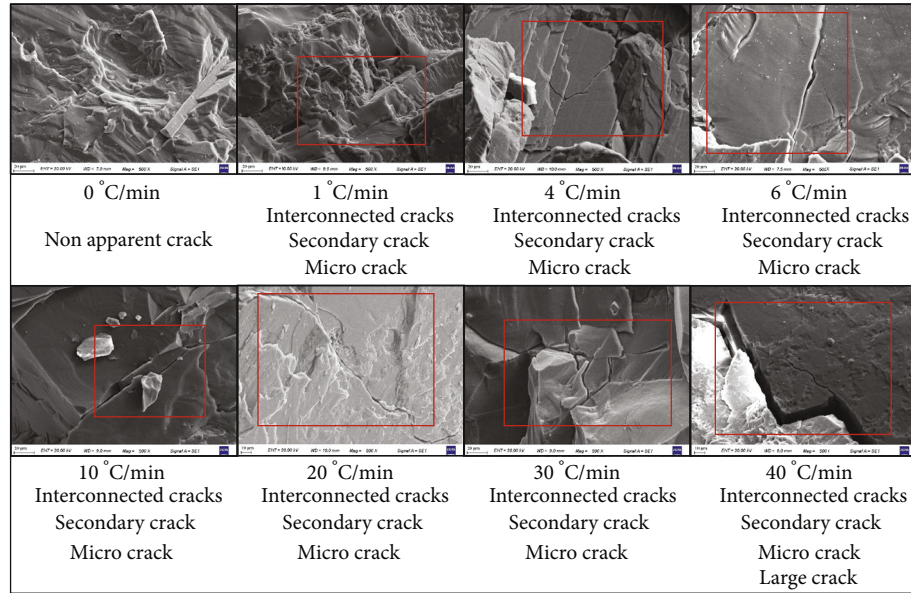
(a)
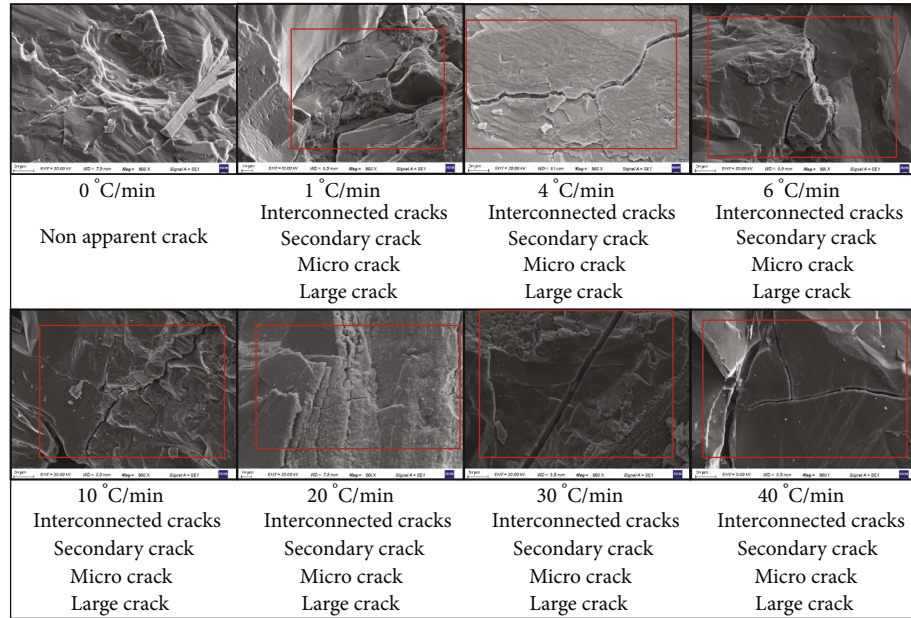
(b)

FIGURE 4: The internal structures of thermal shock treated granite specimens (a) $T = 400°C$ and (b) $T = 600°C$.

specimens could be treated by using different heating methods, and the methods are shown as Figure 3.

Once the target temperature is reached, the temperature is kept constant for 2 hours for the purpose of uniform heating of the specimens, and the specimens are cooled in the heating body slowly to avoid thermal shock. After cooled, the density and ultrasonic wave velocity should be measured. Finally, the internal structure of different thermal shock treated granite specimens could be obtained by using scanning electron microscopy. And the dynamic compressive experiments could be carried out by using the split Hopkinson pressure bar.

For scanning electron microscopy experiment, firstly, the specimen is processed into a cube with dimensions of 10 mm in lengths. Finally, the processed piece could be used for scanning electron microscopy experiment at specified multiplier.

3. Damage Characteristic of Thermal Shock

The macrorupture, loss of stability, and failure of materials are closely related to the distribution of internal cracks and the generation, propagation, and connection of microfractures. Figures 4(a) and 4(b) are the SEM images for internal
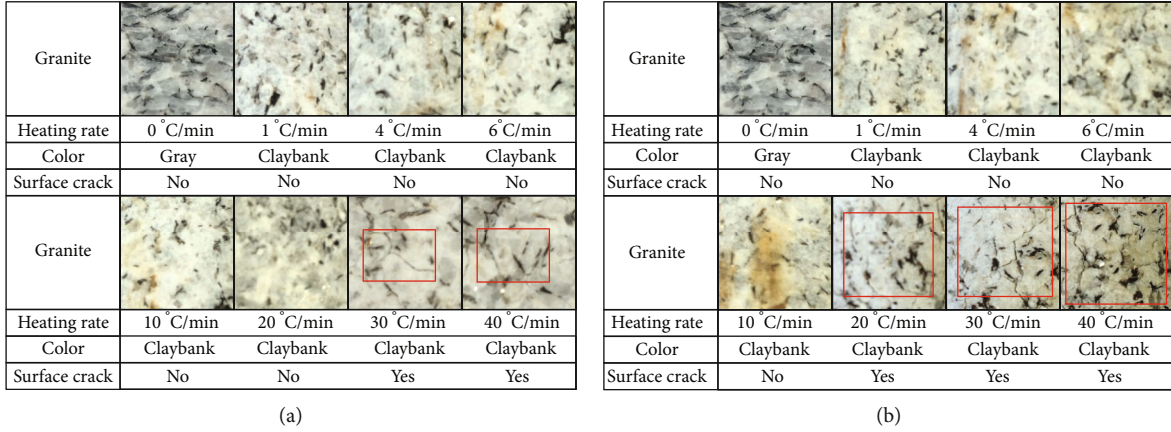
Granite				
Heating rate	0 °C/min	1 °C/min	4 °C/min	6 °C/min
Color	Gray	Claybank	Claybank	Claybank
Surface crack	No	No	No	No
Granite				
Heating rate	10 °C/min	20 °C/min	30 °C/min	40 °C/min
Color	Claybank	Claybank	Claybank	Claybank
Surface crack	No	No	Yes	Yes

(a)

Granite				
Heating rate	0 °C/min	1 °C/min	4 °C/min	6 °C/min
Color	Gray	Claybank	Claybank	Claybank
Surface crack	No	No	No	No
Granite				
Heating rate	10 °C/min	20 °C/min	30 °C/min	40 °C/min
Color	Claybank	Claybank	Claybank	Claybank
Surface crack	No	Yes	Yes	Yes

(b)

Figure 5: The surface appearances of thermal shock treated granite specimens (a) $T = 400°C$ and (b) $T = 600°C$.
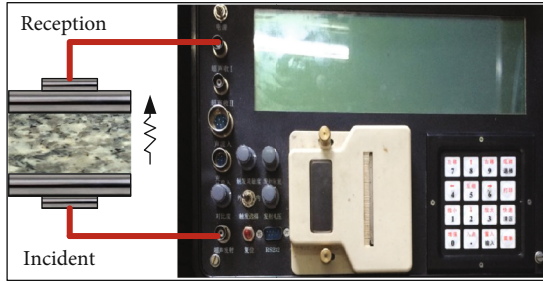

Figure 6: Measurement of ultrasonic wave velocity.

structures of granite specimens heated at different temperatures (400°C and 600°C) and heating rates (1, 4, 6, 10, 20, 30, and 40°C/min), the heating rate of 0°C/min stands for unheated granite specimen, and all the amplifications are 500. Considering on almost the same to internal structures of granite specimens heated at heating rate of 1, 4, and 6°C/min, the images for internal structures of granite specimens, which heated at heating rate of 2°C/min, are not given in Figure 4. As are shown in Figure 4, when the temperature and heating rate increase, different cracks including microcracks, large cracks, secondary cracks, and interconnected cracks appear in the internal structure of granite specimen accordingly, which lies in the difference of the number and size. At 25°C (0°C/min), there is not apparent crack in the view. From 25°C to 600°C, the number and size of cracks increase gradually because of the enlargement of thermal stress which causes by the increasing temperature. At the same temperature whether at 400°C or 600°C, when the heating rate increases from 1 to 6°C/min, the internal structure is almost unchanged, but the number and size of cracks increase as heating rate increases from 6 to 40°C/min. Besides the change of internal structure, the surface appearance also changes to some extent as temperature and heating rate increase. Two obvious changes appear at the surface of specimen when the temperature and heating rate increase, which is the color change and surface crack, as are shown in Figures 5(a) and 5(b). From 25 to 600°C, the color of specimen gradually changes from gray to claybank, especially when the temperature is 600°C, which is conformed to our

previous research [5]. The reasons of color change possibly are the dehydration and oxidation of rocks [31]. Apart from color change, there is another apparent change, namely, surface crack appears with the increasing heating rate. At 400°C, the surface crack appears when the heating rate equals to or is higher than 30°C/min, but at 600°C, it appears when the heating rate equals to or is higher than 20°C/min. Under the same heating rate, the surface cracks appear earlier when the treated temperature is higher. The reasons are there is more defects in the internal of rock specimen at a high temperature.

Damage, which could evaluate the case of the number and size of material internal cracks to some extent, is a macroscopic parameter that represents deterioration degree of material. The larger the number and size of material internal cracks, the larger the damage. Rock materials especially granite, which contains initial defects, such as fissures, pores, and microcracks, under external loads including thermal stresses caused by temperature and thermal shock, could form damage accumulation. The damage accumulation resulting from new born cracks and initial defect propagation may affect the physical and dynamic compressive properties of granite. Due to different propagation velocities of ultrasonic wave in different mediums, simple, and efficient, the method of ultrasonic wave velocity testing is widely adopted in nondestructive testing. In order to quantitative research the damage characteristic of thermal shock and the correlation among damage characteristic, physical, and dynamic compressive properties of granite, damage variable which counts by ultrasonic wave velocity is used here, as shown in Formula (2) [22].

Regardless of the initial damage, which caused by the initial defects, the damage of untreated granite specimen is considered as zero in this paper.

$$D = 1 - \frac{V_n^2}{V_0^2}, \qquad (2)$$

where D is the damage, V_0 is the ultrasonic wave velocity of specimen at 0°C/min, namely, the ultrasonic wave velocity

TABLE 2: Damage (D) of thermal shock treated granite specimens.

| No.	D	No.	D	No.	D	No.	D
D-0-1	0.00	D400-6-2	0.43	D400-40-3	0.80	D600-10-1	0.83
D-0-2	0.00	D400-6-3	0.51	D600-1-1	0.75	D600-10-2	0.83
D-0-4	0.00	D400-10-1	0.60	D600-1-2	0.73	D600-10-3	0.82
D400-1-1	0.48	D400-10-2	0.58	D600-1-3	0.73	D600-20-1	0.90
D400-1-2	0.46	D400-10-3	0.62	D600-2-1	0.74	D600-20-2	0.89
D400-1-3	0.50	D400-20-2	0.76	D600-2-2	0.73	D600-20-3	0.90
D400-2-1	0.47	D400-20-4	0.75	D600-2-3	0.76	D600-30-1	0.94
D400-2-2	0.43	D400-20-5	0.78	D600-4-1	0.75	D600-30-2	0.93
D400-2-3	0.50	D400-30-1	0.80	D600-4-2	0.73	D600-30-4	0.94
D400-4-2	0.49	D400-30-2	0.77	D600-4-3	0.74	D600-40-1	0.96
D400-4-3	0.45	D400-30-3	0.82	D600-6-1	0.74	D600-40-2	0.96
D400-4-4	0.50	D400-40-1	0.84	D600-6-2	0.73	D600-40-5	0.96
D400-6-1	0.47	D400-40-2	0.82	D600-6-3	0.75		
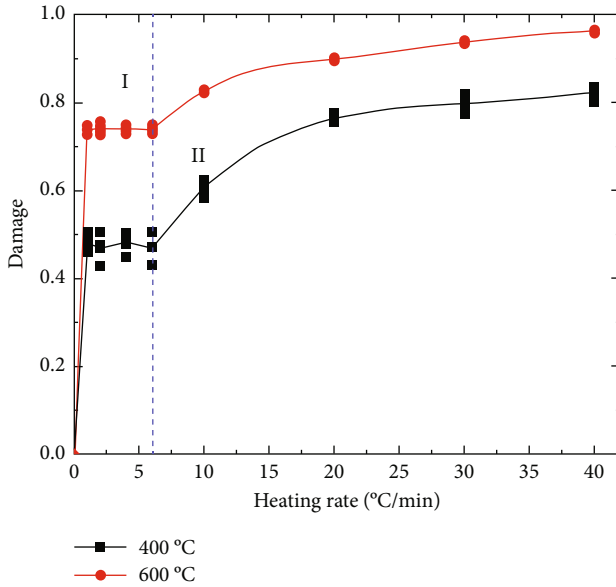
FIGURE 7: The damage of thermal shock treated granite specimens.

of untreated granite specimen, and V_n is the ultrasonic wave velocity of thermal shock treated granite specimen.

The ultrasonic wave velocity is measured before and after thermal shock treatment by using a wave velocity measuring instrument for geotechnical engineering, as shown in Figure 6. By removing high discrete data, the damage of thermal shock treated granite specimens are given in Table 2, the data of which indicates that even at the same temperature the damage is different as heating rate varies, and there is no thermal shock at low heating rate.

Figure 7 shows the correlation between the heating rate and damage of granite specimens at 400°C and 600°C. An obvious phenomenon catches our eyes, in which the relationship between damage and heating rate is divided into two parts (part I and part II) both at 400°C and 600°C. In part I (damage invariant region), the damage almost unchanged when the heating rate increases, which indicates that there is

no thermal shock when the heating rate is smaller than or equals to 6°C/min. The phenomenon confirms to the studies of thermal effect on rock properties, in which they carried out thermal treatment on rock specimens by using heating rate below 5°C/min in order to avoid thermal shock [5, 9, 22, 23, 32, 33]. For example, Yin et al. [5] heated the granite specimen to a target temperature with a heating rate of 2°C/min. At 400°C, when the heating rate is smaller than or equals to 6°C/min and is larger than 0°C/min, the damage is around 0.47 to 0.48, which is resulted from high temperature. When the treated temperature is 600°C, the damage is about 0.74 at heating rate ranging from 0 to 6°C. The water including free and bound water evaporates, and the number and size of internal cracks increases as the temperature increases; therefore, the damage increases accordingly. In part II (damage increasing region), the damage increases gradually with the increasing heating rate both at 400°C and 600°C, that is to say thermal shock appears in this part. The enlargement of thermal stress resulting from thermal shock brings about the increase of the number and size of cracks at the same temperature and finally leads the damage to increase. When the heating rate varies from 10 to 40°C/min, the damage increases from around 0.6 and 0.82 to around 0.82 and 0.96 at 400°C and 600°C, respectively. There is a threshold value between 6°C/min and 10°C/min, which divides the effect of heating rate on the damage characteristic into two parts. Before the threshold value, there is no thermal shock; after that value, the thermal shock appears gradually. Especially, when the heating rate is high, such as 40°C/min, the thermal shock and damage are large.

4. Results and Discussion

4.1. Damage Effect on the Density. By measuring, the density of different thermal treated granite specimens is given in Table 3. When the heating rate is 0°C, namely, the specimen is unheated, the damage is zero, and the density of granite specimen is about 2546.72 kg/m^3. As is shown in Figure 8, before the threshold value, namely, in part I (damage invariant region), the damage is almost unchanged; hence, the density,

TABLE 3: Density (ρ) of different thermal treated granite specimens.

| No.	ρ (kg/m^3)	No.	ρ (kg/m^3)	No.	ρ (kg/m^3)	No.	ρ (kg/m^3)
D-0-1	2546.40	D400-6-2	2517.85	D400-40-3	2500.96	D600-10-1	2483.47
D-0-2	2545.28	D400-6-3	2519.30	D600-1-1	2479.74	D600-10-2	2470.34
D-0-4	2548.47	D400-10-1	2510.70	D600-1-2	2488.36	D600-10-3	2474.59
D400-1-1	2522.72	D400-10-2	2513.80	D600-1-3	2475.22	D600-20-1	2466.42
D400-1-2	2519.41	D400-10-3	2511.30	D600-2-1	2486.24	D600-20-2	2467.53
D400-1-3	2521.53	D400-20-2	2509.03	D600-2-2	2480.13	D600-20-3	2462.25
D400-2-1	2526.12	D400-20-4	2510.36	D600-2-3	2476.45	D600-30-1	2461.20
D400-2-2	2519.03	D400-20-5	2508.59	D600-4-1	2480.41	D600-30-2	2462.93
D400-2-3	2520.44	D400-30-1	2508.72	D600-4-2	2482.95	D600-30-4	2463.05
D400-4-2	2518.74	D400-30-2	2509.68	D600-4-3	2476.85	D600-40-1	2459.72
D400-4-3	2527.85	D400-30-3	2505.54	D600-6-1	2486.74	D600-40-2	2462.51
D400-4-4	2520.93	D400-40-1	2502.07	D600-6-2	2478.53	D600-40-5	2457.55
D400-6-1	2526.57	D400-40-2	2504.65	D600-6-3	2480.25		
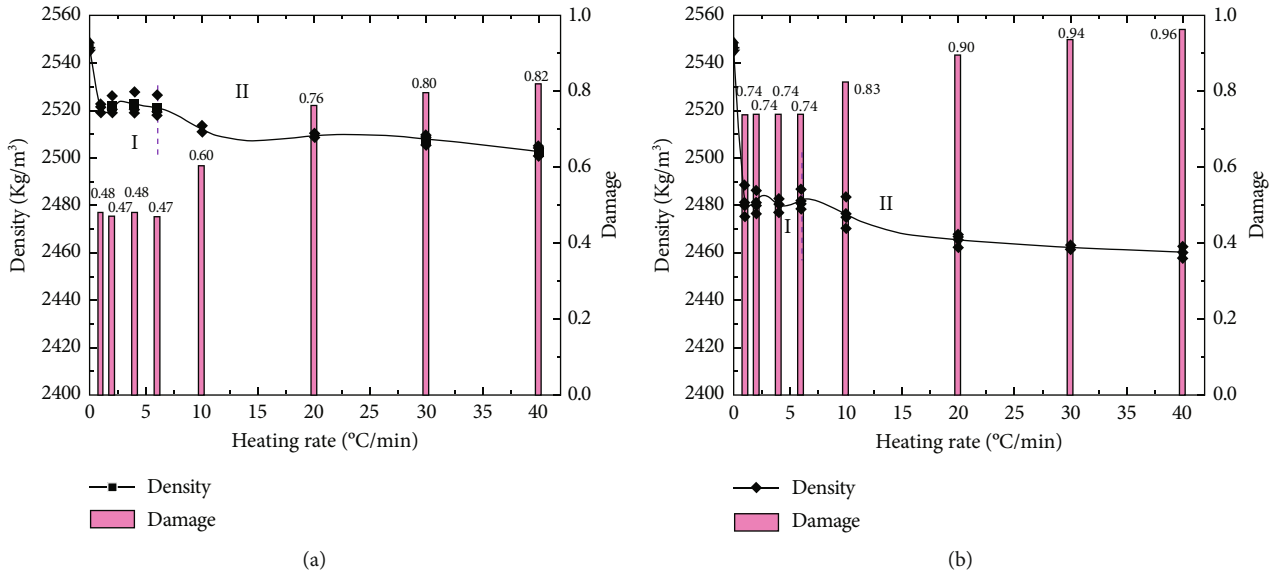
FIGURE 8: Damage effect on the density of thermal shock treated granite specimens (a) $T = 400°C$ and (b) $T = 600°C$.

which is about 2526.13 kg/m^3 at 400°C and 2494.13 kg/m^3 at 600°C, is almost unchanged as heating rate increases. Although density is not too sensitive to temperature, the density decreases to varying degrees accordingly as the temperature increases, and the case is similar to some researches [6, 22, 34]. The reason for the decrease of density is the increase of damage at higher temperature, which due to the water evaporation and the increasing number and size of internal cracks caused by increasing temperature. After the threshold value, in part II (damage increasing region), the thermal stress increases due to the thermal shock, which makes the number and size of cracks to increase, and finally leads to the increase of damage. Therefore, the density decreases accordingly.

4.2. Damage Effect on Dynamic Compressive Properties. For any valid dynamic experiments by using split Hopkinson pressure bar, the experiments should be carried out under the con-

dition of one-dimensional stress and be satisfied with dynamic equilibrium [22]. For the dynamic compressive experiments in the paper, the transmitted stress is roughly the sum of the incident and reflected stresses, as is shown in Figure 9, which indicates that the dynamic stresses on each side of the specimen are balanced. The compressive properties of different thermal shock-treated granite specimens including dynamic compressive strength, σ_d, peak strain, ε_d, and dynamic elastic modulus, E_d, are given in Table 4. The dynamic compressive strength of granite specimen is about 169.66 MPa at 25°C (0°C/min).

4.2.1. Damage Effect on Dynamic Compressive Strength. Dynamic compressive strength, a strength mechanical parameter which could represent the ability to bear dynamic loads, is one of the significant factors to evaluate the structural stability. Considering on the importance of dynamic compressive strength, some researchers have focused on the dynamic
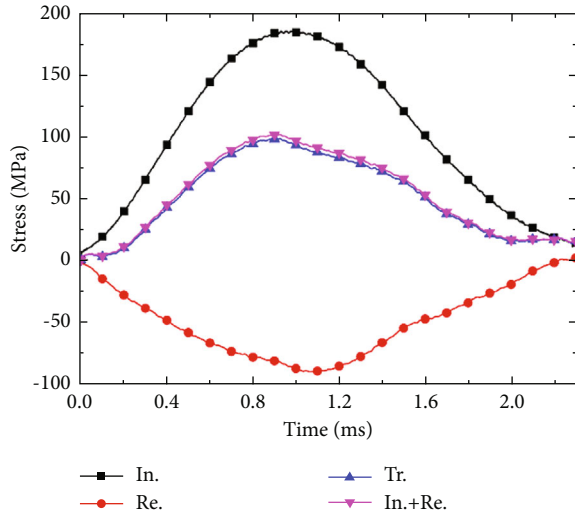
FIGURE 9: Dynamic stress equilibrium of a typical specimen, D600-2-2. (note: in., Re. and Tr. denote the incident, reflected, and transmitted stresses, respectively.)

compressive strength study by carried out laboratory experiments [21, 22, 35]. Figures 10(a) and 10(b) are the damage effect on the dynamic compressive strengths of different thermal treated granite specimens at 400°C and 600°C, respectively. When temperature increases from 25°C to 600°C, due to the increase of damage, the dynamic compressive strength decreases gradually. Similar to many studies, the compressive strength no matter for static or dynamic compressive strength decreases to some degree as temperature increases [1, 4, 5, 22, 34, 36, 37]. At 400°C, before the threshold value (in part I, damage invariant region), because of the unchanged damage as heating rate increases, the dynamic compressive strength is almost constant, around 143.86 MPa. As the heating rate continues to increase, reaches in part II (damage increasing region), the damage increases gradually; thus, the dynamic compressive strength decreases accordingly. 6°C/min-40°C/min, when the damage increases from 0.47 to 0.82, the dynamic compressive strength decreases from 142.92 MPa to 114.99 MPa, a decrease of 27.93 MPa. Similarly, at 600°C, due to the two different parts of damage, the dynamic compressive strength, which is unchanged before the threshold value, is about 104.17 MPa and, after the threshold value the dynamic compressive strength decreases from 104.17 MPa to 71.85 MPa as damage increases from 0.74 to 0.96, a decrease of 32.32 MPa. It shows that the thermal shock damage indeed affects the dynamic compressive strength.

4.2.2. Damage Effect on Dynamic Peak Strain. Dynamic peak strain, a parameter which could reflect deformation extent before peak during the material suffered to dynamic impact, is also one of the important factors that affect the structural stability. As is seen in Figures 11(a) and 11(b), when temperature increases, the ductility enhancement [1, 5], hence, the peak strain increases accordingly. The same to the damage

effect on dynamic compressive strength, during increasing heating rate, the damage effect on the dynamic peak strain is divided into two parts, namely, part I and part II, but some differences still appear. In part I, on account of the almost invariable damage, the peak strain remains constant, nearly 0.60×10^{-2} at 400°C and almost 0.75×10^{-2} at 600°C. In part II, at both 400°C and 600°C, when the heating rate increases, due to the increasing thermal stress caused by thermal shock, the number and size of cracks increase; at this time, the damage increases accordingly and finally leads the dynamic peak strain to increase. After the threshold value, the thermal shock increases as the heating rate increases. When the heating rate increases from 6°C/min to 40°C/min, the damage increases from 0.74 to 0.96; at this moment, the dynamic peak strain increases from 0.60×10^{-2} to 0.85×10^{-2} at 400°C and from 0.75×10^{-2} to 1.20×10^{-2} at 600°C.

4.2.3. Damage Effect on Dynamic Elastic Modulus. Dynamic elastic modulus could represent the elastic deformation capacity of materials under impact loads; meanwhile, it is one of the factors which are important to the structural stability too. Generally, the elastic modulus, both static and dynamic, decreases when temperature increases [1, 4, 5, 22, 36, 37]. Similar to dynamic compressive strength and peak strain, when the heating rate increases, the effect of thermal damage on the dynamic elastic modulus could divided into two parts (part I and part II), as shown in Figures 12(a) and 12(b). Before the threshold value, in part I, whether at 400°C or at 600°C, the dynamic elastic modulus almost remains unchanged due to the unchanged damage value and is about 28.22 GPa and 18.59 GPa, respectively. However, both at 400°C and 600°C, after the threshold value, the dynamic elastic modulus decreases gradually with the rising heating rate because of the increasing damage caused by the increasing thermal shock. At 400°C and 600°C, when the heating rate increases, the dynamic elastic modulus decreases from about 24.36 GPa and 13.59 to 15.64 GPa and 8.75 GPa, almost a decrease of 44.21% and 44.05%, respectively. The dynamic elastic modulus decreases as thermal shock damage increases, which is similar to the thermal effect on dynamic elastic modulus as researchers have stated [20, 22].

By carried out experiments on several igneous rocks treated to 25 to 550°C, Richter et al. [25] enhance that heating rate indeed affects thermal expansion. They discover that if the heating rate is smaller than or equal to 2°C/min and the maximum temperature is smaller than or equal to 250°C, the coefficient of thermal expansion is almost constant. However, when the heating rate is larger than 2°C/min and the temperature is larger than 35°C, new cracks are produced in rock specimen, which leads the coefficient of thermal expansion to decrease. The physical properties, such as the coefficient of thermal expansion, change when heating rate > 2°C/min, which is a little different to our research in this paper. In our research, the threshold value of heating rate is between 6°C/min and 10°C/min, the case is similar to the other researchers who indicate that below 5°C/min, and the

TABLE 4: The compressive properties of thermal shock treated granite specimens.

| No.	$\dot{\varepsilon}$ (s^{-1})	σ_d (MPa)	ε_d (10^{-2})	E_d (GPa)	No.	$\dot{\varepsilon}$ (s^{-1})	σ_d (MPa)	ε_d (10^{-2})	E_d (GPa)
D-0-1	55.12	170.21	0.50	41.64	D400-40-3	62.41	112.30	0.85	15.25
D-0-2	52.34	167.33	0.55	39.89	D600-1-1	62.34	101.75	0.78	17.02
D-0-4	51.89	171.45	0.49	43.24	D600-1-2	65.56	106.25	0.70	19.01
D400-1-1	60.31	145.21	0.65	28.01	D600-1-3	58.21	100.75	0.72	19.95
D400-1-2	55.45	142.55	0.60	29.36	D600-2-1	56.55	107.25	0.77	19.62
D400-1-3	57.01	144.35	0.58	27.92	D600-2-2	58.31	104.33	0.75	18.42
D400-2-1	61.01	146.31	0.62	28.62	D600-2-3	60.45	102.55	0.70	18.42
D400-2-2	55.21	142.55	0.66	27.01	D600-4-1	55.23	104.23	0.74	17.45
D400-2-3	54.45	142.85	0.59	29.25	D600-4-2	57.34	105.71	0.77	19.27
D400-4-2	50.24	142.35	0.60	29.20	D600-4-3	52.15	101.58	0.75	18.50
D400-4-3	56.37	147.21	0.59	27.71	D600-6-1	61.25	108.45	0.73	19.07
D400-4-4	54.23	144.22	0.57	28.56	D600-6-2	60.34	102.95	0.74	17.14
D400-6-1	61.32	145.75	0.56	27.17	D600-6-3	64.21	104.28	0.82	19.19
D400-6-2	60.24	140.56	0.58	28.08	D600-10-1	62.45	97.42	0.86	12.04
D400-6-3	57.45	142.44	0.62	27.79	D600-10-2	55.48	92.25	0.85	13.32
D400-10-1	63.24	135.75	0.71	24.17	D600-10-3	57.34	94.46	0.87	15.41
D400-10-2	60.15	137.85	0.67	24.04	D600-20-1	63.75	84.75	1.01	10.13
D400-10-3	58.45	136.46	0.68	24.86	D600-20-2	65.26	86.24	1.05	9.28
D400-20-2	58.43	125.35	0.75	21.07	D600-20-3	60.45	82.91	1.03	12.93
D400-20-4	52.24	121.45	0.74	19.88	D600-30-1	54.23	74.25	1.14	11.91
D400-20-5	54.45	122.81	0.73	21.34	D600-30-2	59.45	75.64	1.08	7.09
D400-30-1	63.24	118.34	0.81	18.17	D600-30-4	65.56	78.26	1.19	10.92
D400-30-2	65.55	120.25	0.82	18.15	D600-40-1	67.45	72.52	1.18	7.84
D400-30-3	60.21	116.95	0.79	18.06	D600-40-2	68.26	73.24	1.20	8.69
D400-40-1	58.25	115.23	0.87	15.92	D600-40-5	62.55	69.78	1.22	9.72
D400-40-2	65.01	117.45	0.84	15.76					

(note: $\dot{\varepsilon}$ stands for the strain rate.).
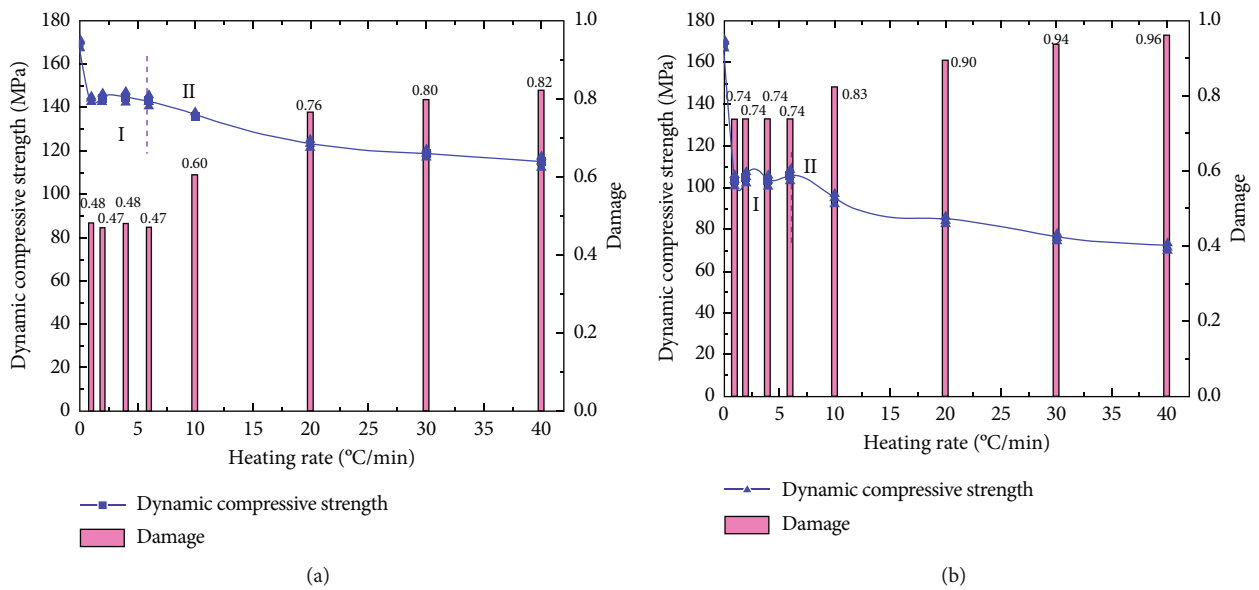
FIGURE 10: Damage effect on the dynamic compressive strength of thermal shock treated granite specimens (a) $T = 400°$C and (b) $T = 600°$C.
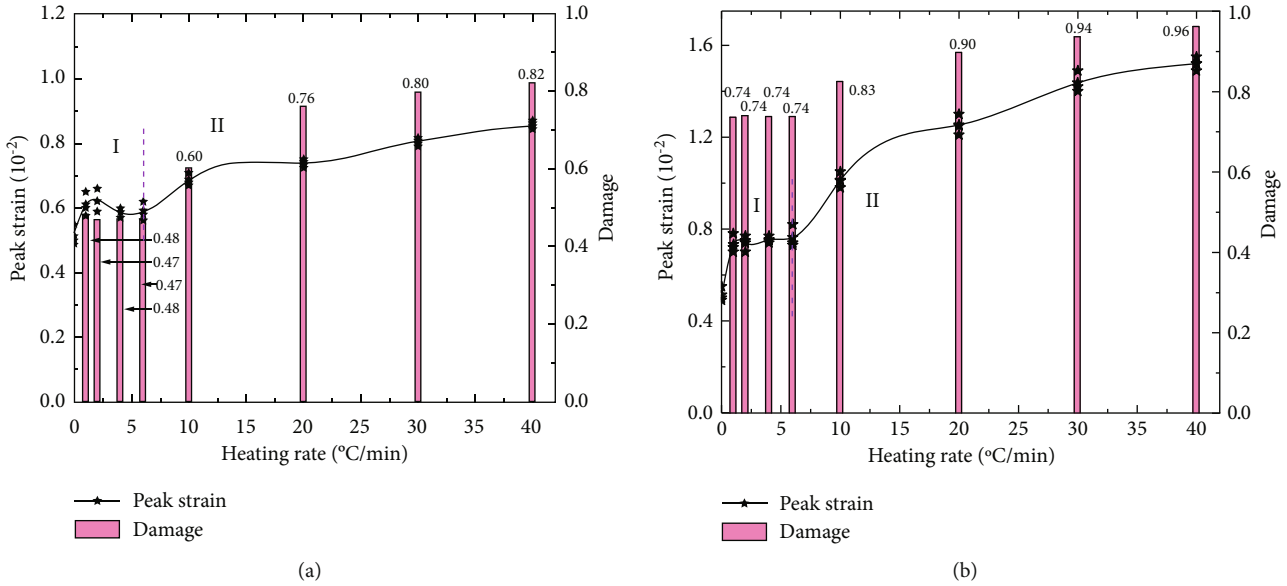
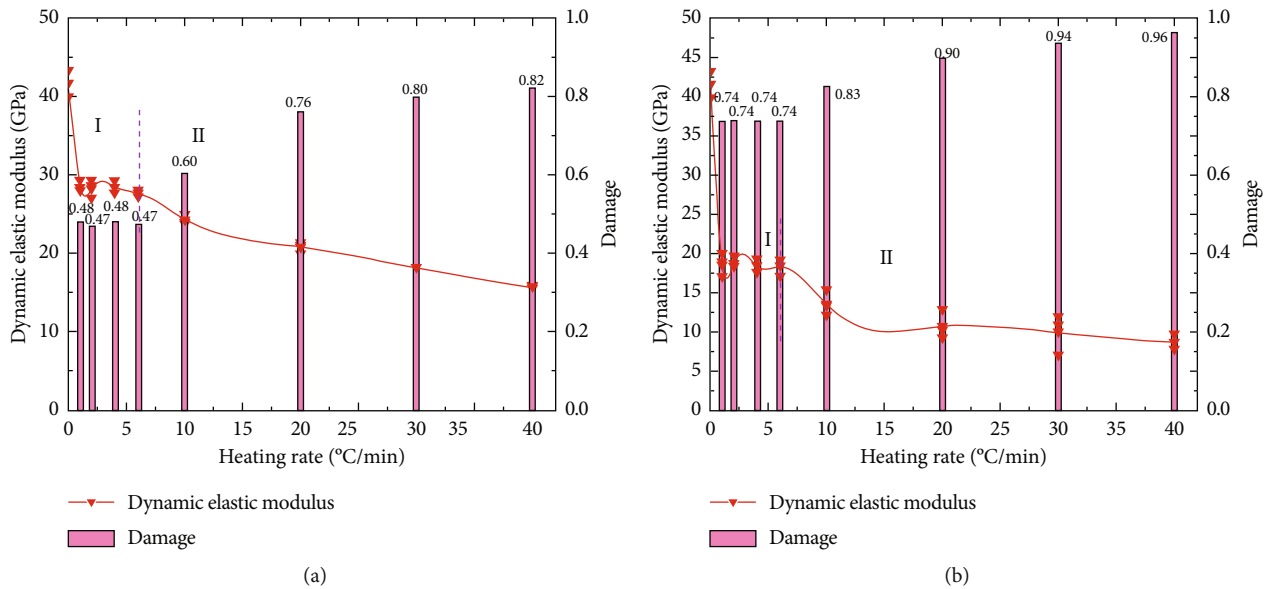FIGURE 11: Damage effect on the peak strain of thermal shock treated granite specimens (a) $T = 400°C$ and (b) $T = 600°C$.

FIGURE 12: Damage effect on the dynamic elastic modulus of thermal shock treated granite specimens (a) $T = 400°C$ and (b) $T = 600°C$.

heating process could avoid thermal shock [5, 9, 22, 23, 32, 33]. The differences may due to the different rock type and components of rocks. In addition, considering on the dynamic compressive properties are all related to thermal shock damage and to obtain the dynamic compressive properties are more different and expensive than thermal shock calculated by ultrasonic wave velocity, we could roughly evaluate the rock structural stability by the means of measure ultrasonic wave velocity to some extent.

The research could provide a theoretical foundation for rock engineering suffered thermal shock, such as geothermal reservoir [38–44].

5. Conclusions

Based on the above results, analysis, and discussion, the conclusions were drawn as follows:

(1) There is a heating rate threshold value between 6 and 10°C/min, and thermal shock appears after the threshold value

(2) The dynamic compressive strength, dynamic elastic modulus, and density decrease accordingly when the thermal shock damage increase, and the opposite phenomenon comes to peak strain

(3) For granite, the method for rock heating by using heating rate below or equal to 6°C/min which could avoid thermal shock

Data Availability

The data used to support the findings of this study are included within the article.

Conflicts of Interest

The authors declared no potential conflicts of interest with respect to the research, authorship, and/or publication of this article.

Acknowledgments

References

[1] X. L. Xu, F. Gao, X. M. Shen, and H. P. Xie, "Mechanical characteristics and microcosmic mechanisms of granite under temperature loads," *Journal of China University of Mining and Technology*, vol. 18, no. 3, pp. 413–417, 2008.

[2] T. J. Yin, Y. J. Chen, X. B. Li, and Q. Li, "Effect of high temperature and strain rate on the elastic modulus of rocks: a review," *International Journal of Earth Sciences*, vol. 110, no. 8, pp. 2639–2660, 2021.

[3] Z. Y. Han, D. Y. Li, T. Zhou, Q. Zhu, and P. G. Ranjith, "Experimental study of stress wave propagation and energy characteristics across rock specimens containing cemented mortar joint with various thicknesses," *International Journal of Rock Mechanics and Mining Sciences*, vol. 131, p. 104352, 2020.

[4] S. Liu and J. Y. Xu, "An experimental study on the physicomechanical properties of two post-high-temperature rocks," *Engineering Geology*, vol. 185, pp. 63–70, 2015.

[5] T. B. Yin, R. H. Shu, X. B. Li, P. Wang, and X. L. Liu, "Comparison of mechanical properties in high temperature and thermal treatment granite," *Transactions of Nonferrous Metals Society of China*, vol. 26, no. 7, pp. 1926–1937, 2016.

[6] H. Tian, T. Kempka, N. X. Xu, and M. Ziegler, "Physical properties of sandstones after high temperature treatment," *Rock Mechanics and Rock Engineering*, vol. 45, no. 6, pp. 1113–1117, 2012.

[7] H. Wu, D. Ma, A. J. S. Spearing, and G. Y. Zhao, "Fracture phenomena and mechanisms of brittle rock with different numbers of openings under uniaxial loading," *Geomechanics and Engineering*, vol. 25, no. 6, pp. 481–493, 2021.

[8] T. B. Yin, L. Bai, X. Li, X. Li, and S. Zhang, "Effect of thermal treatment on the mode I fracture toughness of granite under dynamic and static coupling load," *Engineering Fracture Mechanics*, vol. 199, pp. 143–158, 2018.

[9] S. Shao, P. G. Ranjith, P. L. P. Wasantha, and B. K. Chen, "Experimental and numerical studies on the mechanical behaviour of Australian Strathbogie granite at high temperatures: an application to geothermal energy," *Geothermics*, vol. 54, no. 54, pp. 96–108, 2015.

[10] F. E. Heuze, "High-temperature mechanical, physical and thermal properties of granitic rocks– a review," *International Journal of Rock Mechanics and Mining Sciences and Geomechanics Abstracts*, vol. 20, no. 1, pp. 3–10, 1983.

[11] C. F. Tsang, "Linking thermal, hydrological, and mechanical processes in fractured rocks," *Annual Review of Earth and Planetary Sciences*, vol. 27, no. 1, pp. 359–384, 1999.

[12] W. G. Liang, S. G. Xu, and Y. S. Zhao, "Experimental study of temperature effects on physical and mechanical characteristics of salt rock," *Rock Mechanics and Rock Engineering*, vol. 39, no. 5, pp. 469–482, 2006.

[13] M. Hajpál, "Changes in sandstones of historical monuments exposed to fire or high temperature," *Fire Technology*, vol. 38, no. 4, pp. 373–382, 2002.

[14] D. M. Freire-Lista, R. Fort, and M. J. Varas-Muriel, "Thermal stress-induced microcracking in building granite," *Engineering Geology*, vol. 206, pp. 83–93, 2016.

[15] V. Brotóns, R. Tomás, S. Ivorra, and J. C. Alarcón, "Temperature influence on the physical and mechanical properties of a porous rock: San Julian's calcarenite," *Engineering Geology*, vol. 167, pp. 117–127, 2013.

[16] H. Yavuz, S. Demirdag, and S. Caran, "Thermal effect on the physical properties of carbonate rocks," *International Journal of Rock Mechanics and Mining Sciences*, vol. 47, no. 1, pp. 94–103, 2010.

[17] R. H. Shu, T. B. Yin, X. B. Li, Z. Q. Yin, and L. Z. Tang, "Effect of thermal treatment on energy dissipation of granite under cyclic impact loading," *Transactions of Nonferrous Metals Society of China*, vol. 29, no. 2, pp. 385–396, 2019.

[18] T. B. Yin, S. S. Zhang, X. B. Li, and L. Bai, "Evolution of dynamic mechanical properties of heated granite subjected to rapid cooling," *Geomechanics and Engineering*, vol. 16, no. 5, pp. 483–493, 2018.

[19] T. B. Yin, S. S. Zhang, X. B. Li, and L. Bai, "A numerical estimate method of dynamic fracture initiation toughness of rock under high temperature," *Engineering and Fracture Mechanics*, vol. 204, pp. 87–102, 2018.

[20] S. Liu and J. Xu, "Study on dynamic characteristics of marble under impact loading and high temperature," *International Journal of Rock Mechanics and Mining Sciences*, vol. 62, no. 5, pp. 51–58, 2013.

[21] S. Huang and K. W. Xia, "Effect of heat-treatment on the dynamic compressive strength of Longyou sandstone," *Engineering Geology*, vol. 191, pp. 1–7, 2015.

[22] T. B. Yin, R. H. Shu, X. B. Li, P. Wang, and L. J. Dong, "Combined effects of temperature and axial pressure on dynamic mechanical properties of granite," *Transactions of Nonferrous Metals Society of China*, vol. 26, no. 8, pp. 2209–2219, 2016.

[23] T. B. Yin, P. Wang, X. B. Li, B. Wu, M. Tao, and R. Shu, "Determination of dynamic flexural tensile strength of thermally treated Laurentian granite using semi-circular specimens," *Rock Mechanics and Rock Engineering*, vol. 49, no. 10, pp. 3887–3898, 2016.

[24] K. Thirumalai and S. G. Demou, "Effect of reduced pressure on thermal-expansion behavior of rocks and its significance to thermal fragmentation," *Journal of Applied Physics*, vol. 41, no. 13, pp. 5147–5151, 1970.

[25] D. Richter and G. Simmons, "Thermal expansion behavior of igneous rocks," *International Journal of Rock Mechanics and Mining Science and Geomechanics Abstracts*, vol. 11, no. 10, pp. 403–411, 1974.

[26] C. Yong and C. Wang, "Thermally induced acoustic emission in Westerly granite," *Geophysical Research Letters*, vol. 7, no. 12, pp. 1089–1092, 1980.

[27] M. Li, X. B. Mao, L. L. Cao, H. Pu, and A. Lu, "Influence of heating rate on the dynamic mechanical performance of coal measure rocks," *International Journal of Geomechanics*, vol. 17, no. 8, p. 04017020, 2017.

[28] Y. X. Zhou, K. W. Xia, X. B. Li et al., "Suggested methods for determining the dynamic strength parameters and mode-I fracture toughness of rock materials," *International Journal of Rock Mechanics and Mining Sciences*, vol. 49, pp. 105–112, 2012.

[29] X. B. Li, T. Lok, J. Zhao, and P. J. Zhao, "Oscillation elimination in the Hopkinson bar apparatus and resultant complete dynamic stress-strain curves for rocks," *International Journal of Rock Mechanics and Mining Sciences*, vol. 37, no. 7, pp. 1055–1060, 2000.

[30] I. Ohno, "Temperature variation of elastic properties of .ALPHA.-Quartz up to the .ALPHA.-.BETA. transition," *Journal of Physics of the Earth*, vol. 43, no. 2, pp. 157–169, 1995.

[31] M. Hajpál and Á. Török, "Mineralogical and colour changes of quartz sandstones by heat," *Environmental Geology*, vol. 46, no. 3-4, pp. 311–322, 2004.

[32] S. Q. Yang, P. G. Ranjith, H. W. Jing, W. L. Tian, and Y. Ju, "An experimental investigation on thermal damage and failure mechanical behavior of granite after exposure to different high temperature treatments," *Geothermics*, vol. 65, pp. 180–197, 2017.

[33] Q. L. Ding, F. Ju, X. B. Mao, D. Ma, B. Y. Yu, and S. B. Song, "Experimental investigation of the mechanical behavior in unloading conditions of sandstone after high-temperature treatment," *Rock Mechanics and Rock Engineering*, vol. 49, no. 7, pp. 2641–2653, 2016.

[34] P. K. Gautam, A. K. Verma, M. K. Jha, P. Sharma, and T. N. Singh, "Effect of high temperature on physical and mechanical properties of Jalore granite," *Journal of Applied Geophysics*, vol. 159, pp. 460–474, 2018.

[35] S. J. Bauer, B. Song, and B. Sanborn, "Dynamic compressive strength of rock salts," *International Journal of Rock Mechanics and Mining Sciences*, vol. 113, pp. 112–120, 2019.

[36] R. D. Dwivedi, R. K. Goel, V. V. R. Prasad, and A. Sinha, "Thermo-mechanical properties of Indian and other granites," *International Journal of Rock Mechanics and Mining Sciences*, vol. 45, no. 3, pp. 303–315, 2008.

[37] Y. L. Chen, J. Ni, W. Shao, and R. Azzam, "Experimental study on the influence of temperature on the mechanical properties of granite under uni-axial compression and fatigue loading," *International Journal of Rock Mechanics and Mining Sciences*, vol. 56, pp. 62–66, 2012.

[38] X. Liang, P. Hou, Y. Xue, X. J. Yang, F. Gao, and J. Liu, "A fractal perspective on fracture initiation and propagation of reservoir rocks under water and nitrogen fracturing," *Fractals-Complex Geom Patterns and Scaling in nature and Society*, vol. 29, no. 7, p. 2150189, 2021.

[39] P. Hou, X. Liang, F. Gao, J. Dong, J. He, and Y. Xue, "Quantitative visualization and characteristics of gas flow in 3D pore-fracture system of tight rock based on Lattice Boltzmann simulation," *Journal of Natural Gas Science and Engineering*, vol. 89, p. 103867, 2021.

[40] P. Hou, X. Liang, Y. Zhang, J. He, F. Gao, and J. Liu, "3D multi-scale reconstruction of fractured shale and influence of fracture morphology on shale gas flow," *Natural Resources Research*, vol. 30, no. 3, pp. 2463–2481, 2021.

[41] X. Liang, P. Hou, X. J. Yang et al., "On estimating plastic zones and propagation angles for mixed mode I/II cracks considering fractal effect," *Fractals-Complex Geometry Patterns and Scaling in Nature and Society*, vol. 30, no. 1, 2022.

[42] P. Hou, S. J. Su, X. Liang et al., "Effect of liquid nitrogen freeze-thaw cycle on fracture toughness and energy release rate of saturated sandstone," *Engineering Fracture Mechanics*, vol. 258, p. 108066, 2021.

[43] J. Liu, Y. Xue, W. Chen, P. Hou, S. Wang, and X. Liang, "Variational phase-field model based on lower-dimensional interfacial element in FEM framework for investigating fracture behavior in layered rocks," *Engineering Fracture Mechanics*, vol. 255, p. 107962, 2021.

[44] J. Liu, Y. Xue, Q. Zhang, H. Wang, and S. Wang, "Coupled thermo-hydro-mechanical modelling for geothermal doublet system with 3D fractal fracture," *Applied Thermal Engineering*, vol. 200, p. 117716, 2022.